

# SEM melt track analysis

Mack Sowers MSE130

Fall 2023 Lab 2: Laser melting of 304SS

QUANTITATIVE ANALYSIS OF MICROSTRUCTURE	2
TRANSLATION VELOCITY	3
UNKNOWN THERMAL GRADIENT	4
LINEAR ENERGY DENSITY	5
QUALITATIVE ANALYSIS	7
PRIMARY PHASE OF SOLIDIFICATION	7
CONVECTION BANDING AT HIGH LINEAR ENERGY DENSITY	8
VAPOR CONVECTION AND THE KEYHOLE	10
VALIDITY OF PLANE FRONT STABILITY CRITERION	12

## QUANTITATIVE ANALYSIS OF MICROSTRUCTURE

At the top of the melt track, directly under the laser, and at the top left of the fusion line, the spacing of cells and dendrites was carefully measured. These locations were chosen in order to make some assumptions that allowed further analysis.

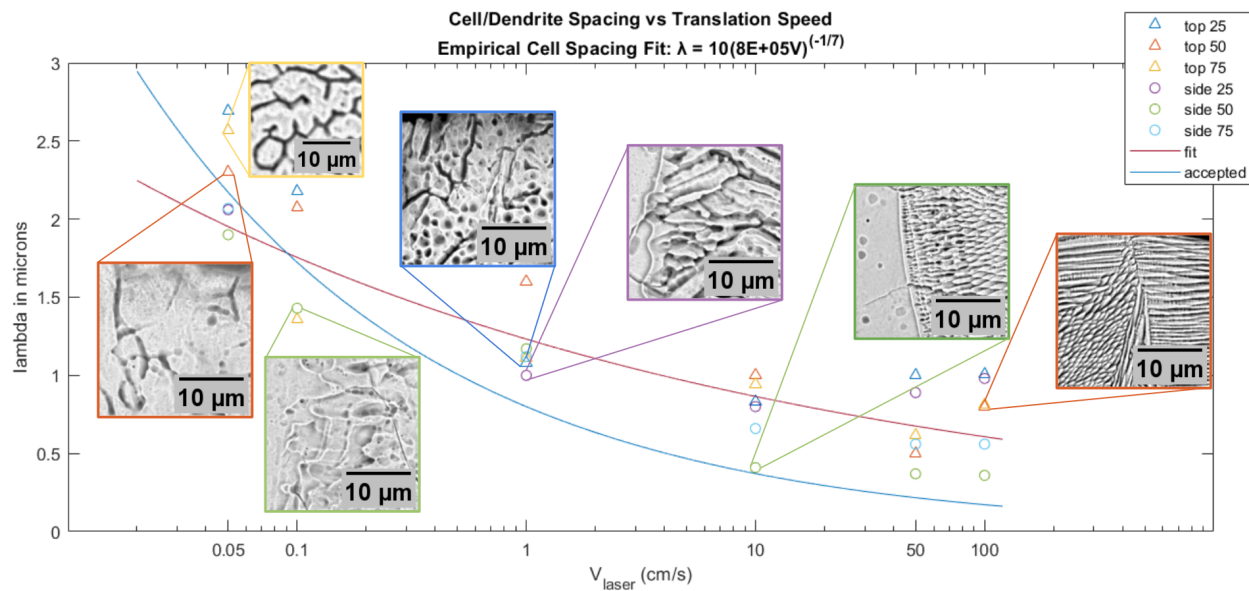


Figure 1: The plot of cell and dendrite spacing vs laser translation speed shows that this spacing decreases at higher translation speeds. A selection of images associated with specific data points show that not only do cells become closer to each other, they become more ordered. The plot also uses the form of the empirical cell spacing fit to show the trend. The red line is a fit, while the blue line uses an arbitrary G.

The cooling rate was calculated from the cell spacing, as  $\lambda = 80(CR)^{-\frac{1}{3}}$ . The figure plotting cell spacing vs translation speed shows that the empirical formula used doesn't generally work well as a function of translation speed. The blue line represents this formula with an arbitrary choice of G=10,000,000 degrees C/cm. The general shape of the trend as well change in spacing can easily be seen as a function of velocity in some way.

For data taken on the surface, the velocity of the laser will be similar to that of solidification. Assuming for a moment that this is a fair assumption, it is possible to consider how well the samples match the expected microstructure. G/V determines the morphology of the structure and GV or the cooling rate, determines the size of the structure where a lower cooling rate gives a larger structure, whereas a low G/R indicates a

dendritic structure. Plotting calculated cooling rates using  $G = V^{-1}(\frac{\lambda_{\mu m}}{80})^{-3}$  as well as the criterion for solidification mode  $\text{constitutional supercooling} = \frac{G}{V} \geq -\frac{m_L}{D_L} Co(\frac{1}{k} - 1)$  on the GV axis is efficient for this analysis as these two parameters dominate the solidification behavior in well behaved conduction-only systems.

In the plot 'G vs V at surface...' the average cooling rate (of the 25%, 50%, and 75% locations) for the surface of each track is shown as a constant value as a function of V in order to show the change in dendrite size. Each data point from the surface was plotted with the same formula, but using the translation velocity instead of a range of V.

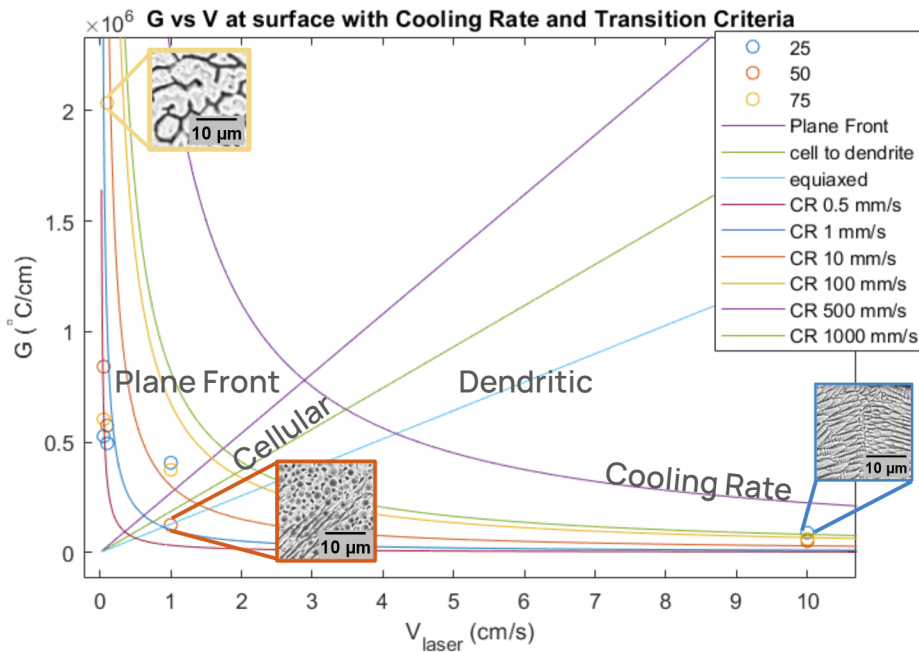


Figure 2: Plot of local G and translation Velocity with lines of constant cooling rate, and showing the calculated cooling rate for each surface data point by approximating solidification velocity at the surface to be V<sub>laser</sub>.

## TRANSLATION VELOCITY

The solidification velocity is only a component of the translation velocity. Although surface measurements were taken as close as possible to the surface of the melt track where the velocity is at a maximum, even those local velocities are not guaranteed to fully embody the translation speed. The G vs V at surface plot highlights the fact that eight of the data points show a G/V that indicates a plane front morphology as they are left of the G/V criterion line, shown in purple. An image from the surface of the 1mm/s track at 75%

translation is shown on the plot as a thumbnail outlined in yellow. The morphology is confusing but does not appear to be plane front. The three tracks with the fastest translation are solidly in the dendritic region. A thumbnail in blue shows the 100mm/s 25% translation surface with the anticipated fine dendrite structure. The faster tracks have been cropped out of the photo but they also lie on the lower right of the plot. One lower speed cross section, 10 mm/s at 50% translation, has a supposed G/V that indicates dendritic rather than plane front, and it is shown on the plot with an orange outline. The image is hard to interpret as it looks to be a mixture of phases and phenomena. The mode of solidification observed in the images is almost always dendritic due to the extreme conditions, and otherwise cellular. In the analysis of the relationship between cell spacing and translation velocity, there are a number of factors to consider. Deviations from the model will be considered qualitatively in the 'Qualitative Analysis' section.

#### UNKNOWN THERMAL GRADIENT

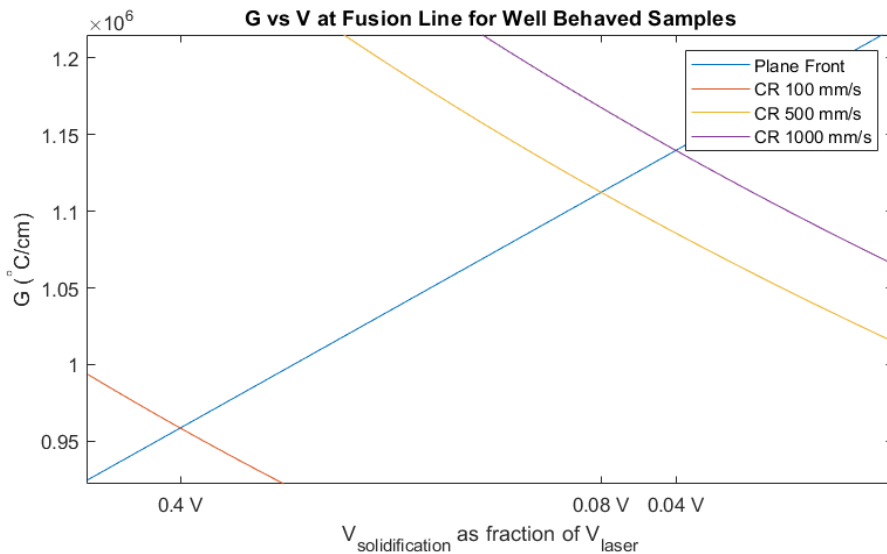


Figure 3: G vs V plot for the fusion line cooling rates, showing how the average solidification velocity for each track is calculated.

At the surface, maximum velocity corresponds to minimum thermal gradient, and estimating the velocity allowed extrapolation of an unknown surface G value. However the fusion line has a maximum thermal gradient, and a minimum local solidification velocity, and the approximation is no longer warranted. The ratio between the thermal gradient, G,

and the solidification velocity,  $V$ , is usually large enough for plane front solidification at the fusion line, if only for a fraction of a micron away from the base metal. Measuring the cell spacing as close as possible to the plane front justifies the use of

$$\text{constitutional supercooling} = \frac{G}{V} \geq -\frac{m_L}{D_L} C_O \left( \frac{1}{k} - 1 \right) \text{ to approximate the local solidification velocities,}$$

where  $G(V)$  for plane front intersects the cooling rate curves. Solidification velocities should not exceed translation velocity. For the 100, 500, and 1000mm/s tracks, the avg fusion line solidification velocity was found to be less than half of the translation velocity for the track. Since local  $V$  should be a minimum at the fusion line, the results for the 500 and 1000 mm/s track are promising, with 8% and 4% of translation velocity respectively.

## LINEAR ENERGY DENSITY

Plotting in terms of energy density rather than translation velocity is more valuable when comparing to other experiments, and it reduces some of the confusion between the two different velocities.

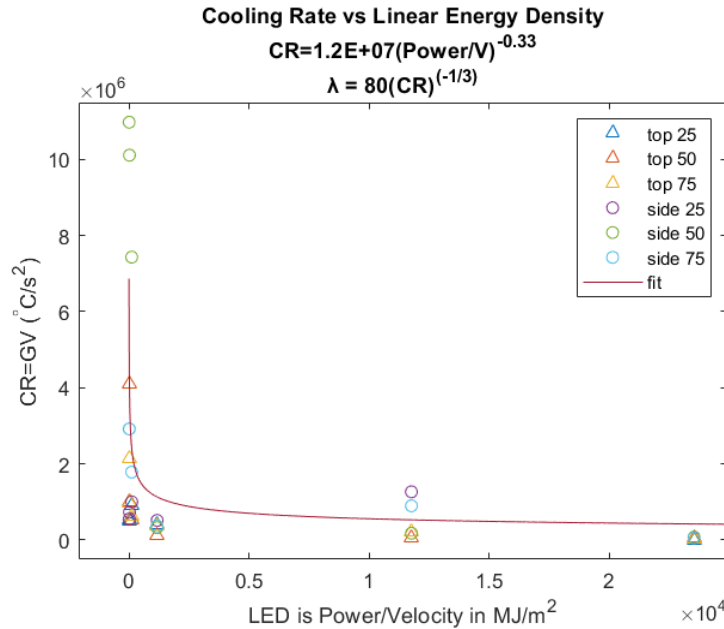


Figure 4: The cooling rate, calculated according to the empirical formula stated on the plot, against the linear energy density. The fit to the dataset is similarly to the  $-1/3$  power.

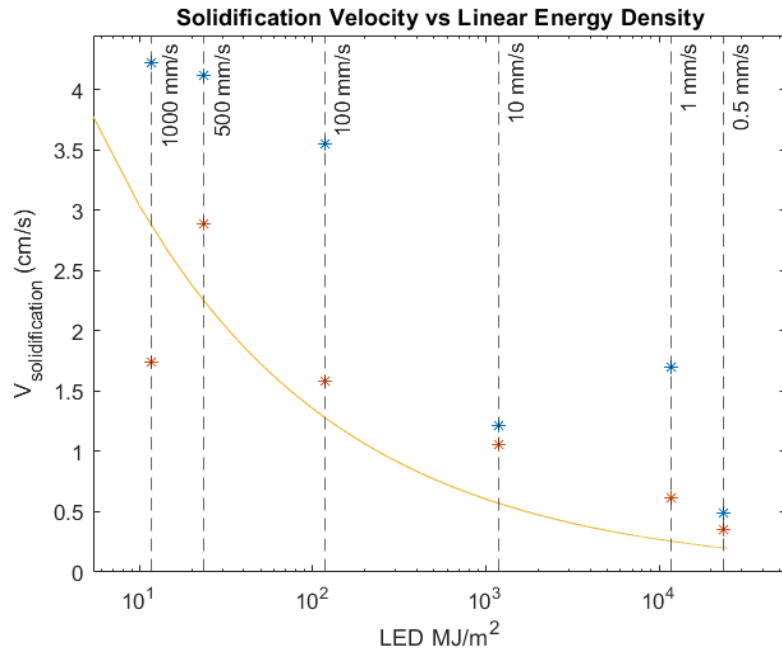


Figure 5: Plot of solidification velocity vs linear energy density, with a general trend supported by the fit for the same parameters as in the 2019 paper by Bertoli et al.

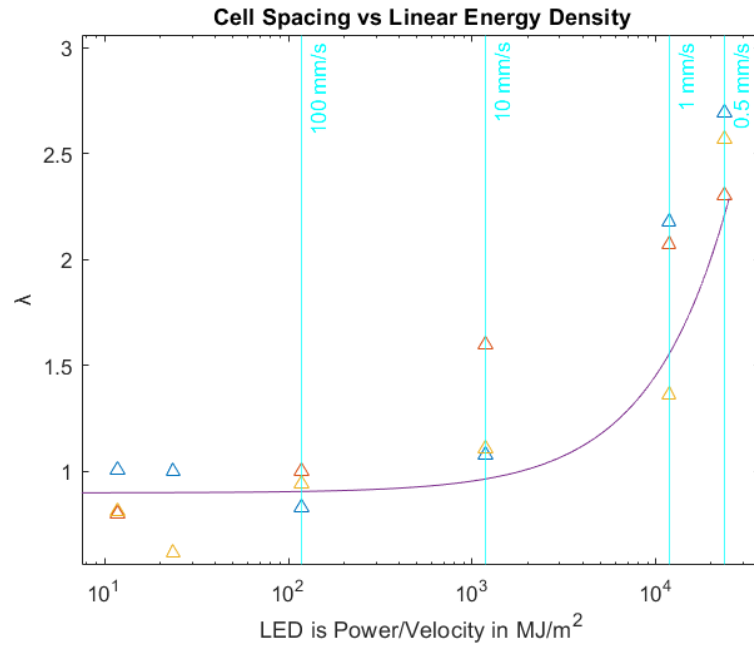


Figure 6: Plot of cell spacing vs linear energy density with a fit to the data.

## QUALITATIVE ANALYSIS

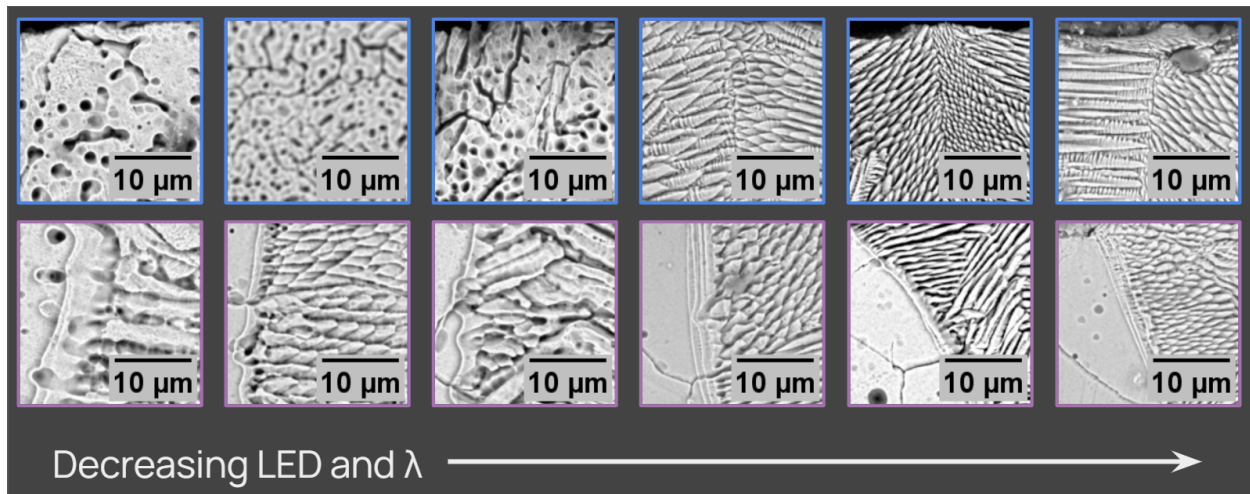


Figure 7: Regions analyzed for all 6 laser velocities at 25% translation. Top: Surface. Bottom: fusion at upper left. By choosing the same location in each sample, the change in phase and feature size is readily apparent. The 3 highest translation speeds are on the left; 100, 500, and 1000 mm/s tracks show well ordered austenitic dendrites. Conversely, from the left the .5, 1, and 10 mm/s track are shown to have a higher degree of disorder, larger features, and a mix of phases.

## PRIMARY PHASE OF SOLIDIFICATION

In many cases it is easy to identify the primary phase of solidification: clear white dendrites on a black background are austenitic, whereas holes on a substrate of white are ferritic. Figure 7 shows an increase in austenitic structures with decreasing linear energy density. This clear difference is due to ferrite being etched away during the nitric acid treatment, causing the ferritic regions to appear dark relative to the concentration. Plane front is generally only seen where it is an obvious white line along fusion lines and occasionally in banding, as discussed in the section: Convection Banding at High Linear Energy Density. The distribution of solute is sensitive to both temperature and speed of solidification. At steady state, the thermodynamically stable material is primary-ferrite dominant. Additional quantitative analysis outside the scope of this report could be done on a specified

---

composition of ferritic-austenitic mode 304SS to calculate the expected phase fractions at the given power densities and cooling rates, using ThermoCalc software, the Schiel Gulliver model for rapid cooling, as well as other kinetic models. The SEM images could also be measured to some degree of accuracy for phase fraction observed, and compared to the calculated predictions. The purpose of this analysis would be to confirm what is already qualitatively apparent. Those observations, limited to the 200W laser, will be discussed here.

The primary phase to solidify in this system is ferrite, which proceeds to transition into austenite during cooling in this fashion:  $L \rightarrow L+\delta \rightarrow L+\delta+y \rightarrow \delta+y \rightarrow y$ . However rapid solidification velocities lead to metastable austenitic dendrite growth. It is additionally apparent that the higher linear energy density, inversely proportional to translation speed, would create a larger temperature gradient, as can be extrapolated from figures 2 and 5.

The 25% translation cross sections were requested as the subject of analysis. Figure 7 shows the areas of that subset that were used for quantitative analysis. Below, all samples shown are from the 25% translation subset. The 100, 500, and 1000 mm/s tracks show well ordered austenitic dendrites, as depicted in figure 7. Conversely, from the left the .5, 1, and 10 mm/s track are shown to have a higher degree of disorder, larger features, and a mix of phases. Correlated with this is the appearance of convection.

#### **CONVECTION BANDING AT HIGH LINEAR ENERGY DENSITY**

Convection creates a mixture of cooling rates, temperature gradients, and solidification velocities, which leads to a set of microstructures that are interesting and difficult to analyze. The image shown in figure 8 shows a circular feature that is likely to be a void caused by trapped vapor during convection. There are changes in shape and density of solute that suggest a mix of phases, as it is unclear what composition is solidifying first due to the lack of ordered and obvious cells. The context for the supposed void is shown in figure 9. It appears that there is convection that flows out towards the side, down, and then up through the center, due to the shape of the surface. The area directly under the laser is raised for this track indicating the surface tension is higher there even though that location is hottest, which indicates the direction. The convection bands can be identified by the change in solute distribution, which is the direct result of changes in temperature gradient and solidification velocity caused by the agitation.

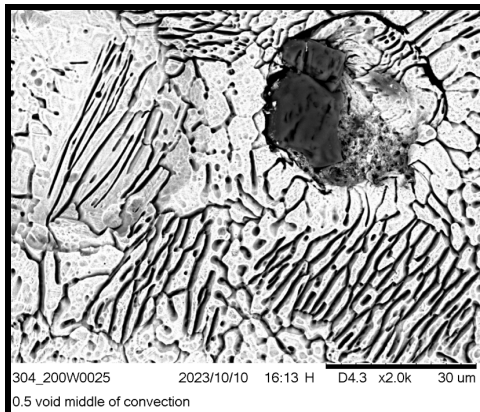


Figure 8: A feature within the 25% track cross section of the highest energy density track analyzed; the 0.5 mm/s laser speed. The feature appears to be a void within a mixed phase matrix.

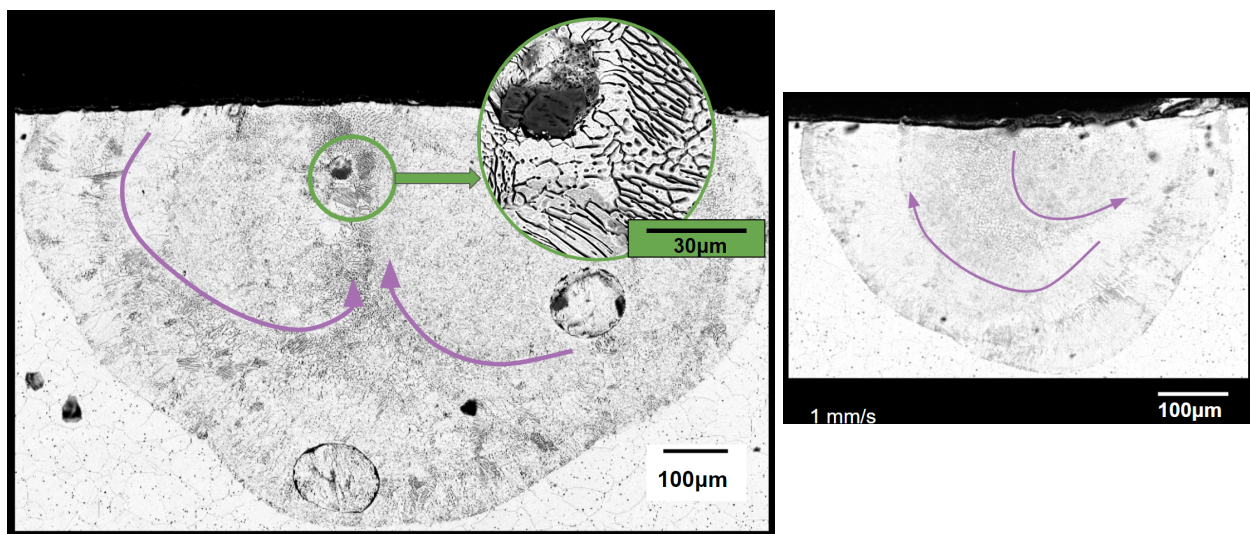


Figure 9: Full cross section of Left: 0.5 mm/s and Right: 1mm/s translation speed and 25% translation of track length. This figure depicts the context for figure 8 and 10: a void between convection bands, and proposed convection. The direction of convection is indicated with curved purple arrows.

At 1mm/s translation speed, the cross section shows a more standard Marangoni effect where the edge of the melt track is raised due to higher surface tension. In figure 9, proposed directions of convection are superimposed over the first couple convection bands. The segment of the fusion line used for analysis (see figure 7) appears to be less affected by the aggressive amount of convection, possibly because it is slightly outside of the curve of the outermost band as depicted in figure 9, and as such the area clearly experienced less solute redistribution. The very top of the fusion line was chosen on the supposition that the location would be less affected, intuitively, and as such would better fit

---

the equations that are based on convection only models. From that point, the intuition might be justified.

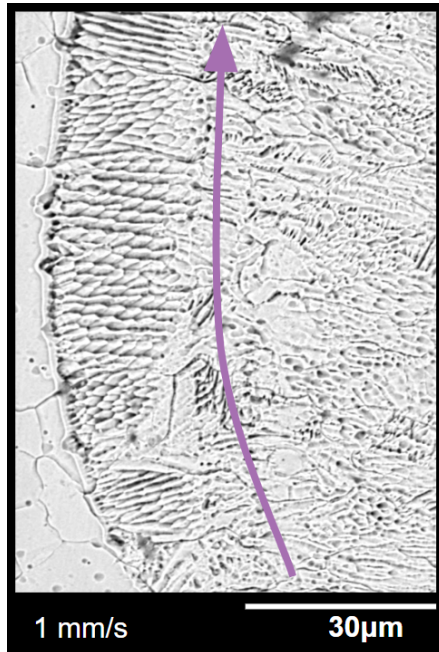


Figure 10: Proposed motion of convection that would allow ordered growth of austenitic dendrites along the fusion line in one location of the 1mm/s cross section, which was used for quantitative analysis. This area extrudes out to the side and may have been out of the main streams of convection.

In figure 10, dendrites grow in many directions. Notably, those growing mostly in plane with the cross section aren't only perpendicular to the fusion line, they also appear to be growing away from the convection band. This may be indicative of a high thermal gradient caused by convection.

#### VAPOR CONVECTION AND THE KEYHOLE

Vapor convection is the cause of the keyhole feature; the upper part of the cross section resembles a pure conduction mode for solidification. Again, the choice to quantitatively analyze the fusion line next to the surface is based on the intuition that there will be more solute distribution in features that are created from convection; looking at figure 11 it can be inferred that the mechanisms for solidification along the keyhole vary highly with location, even along the fusion line. It's not only the keyholes that have features indicative of vapor convection though. The 1 and 10 mm/s cross sections carried characteristics seen in both the fast and slow translation speeds. Figure 12 compares two vapor convection tips.

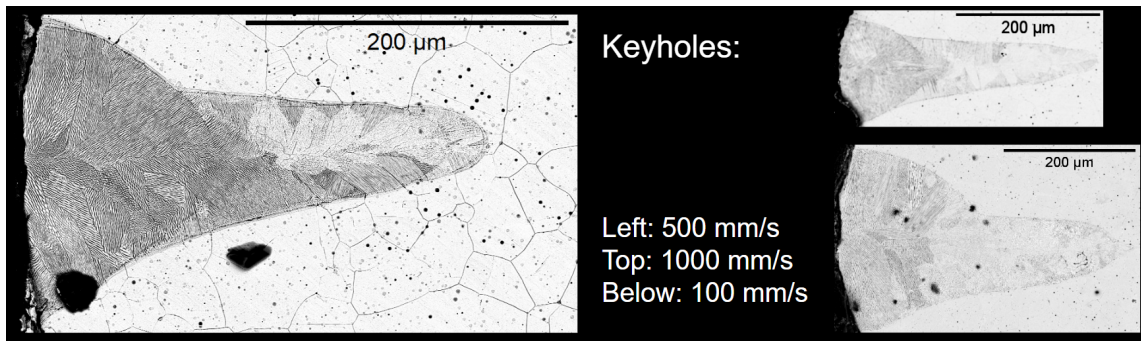


Figure 11: The full cross sections of 25% translation along 100 mm/s, 500 mm/s, and 1000 mm/s (counter clockwise from the lower right corner, as labeled in the image) showing the characteristic shape of “keyhole”.

Vapor convection creates a clear redistribution of solute at the lower tip of the melt, which creates characteristic banding. This can look ghost-like because the chromium rich solute that etches black is swept away, but the plane front that solidified is bright white and remains. This is evident even in the lower resolution image of the 10 mm/s track shown in figure 12, because some of the initially formed ferrite remains as well, creating contrast.

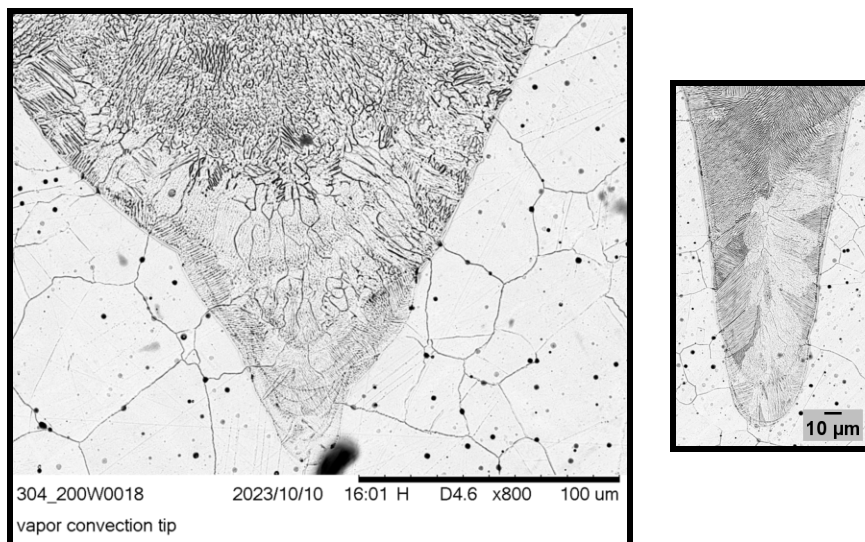


Figure 12: Left: 10 mm/s and right: 500mm/s. Although the size and shape of the melt cross-sections is vastly different, they both show the convection banding and light color from solute redistribution that is characteristic of vapor convection.

The microstructure at the tip of a keyhole is shown in figure 13 using the 500 mm/s and 1000 mm/s melt tracks. It is noteworthy that the grain structure of the substrate apparently affects the re-solidification, as the etch indicates. On the left side of both images in figure

13, a dark line begins in the base metal and appears to continue into the rapid solidification structure. Chromium diffuses to grain boundaries, and is etched by the nitric acid, but there is no other obvious reason for the solute diffusion to create the line within the melt, so it stands to reason that this is a continuation of the grain. Analysis of the effect the grain orientation has on resolidification is outside the scope of this report.

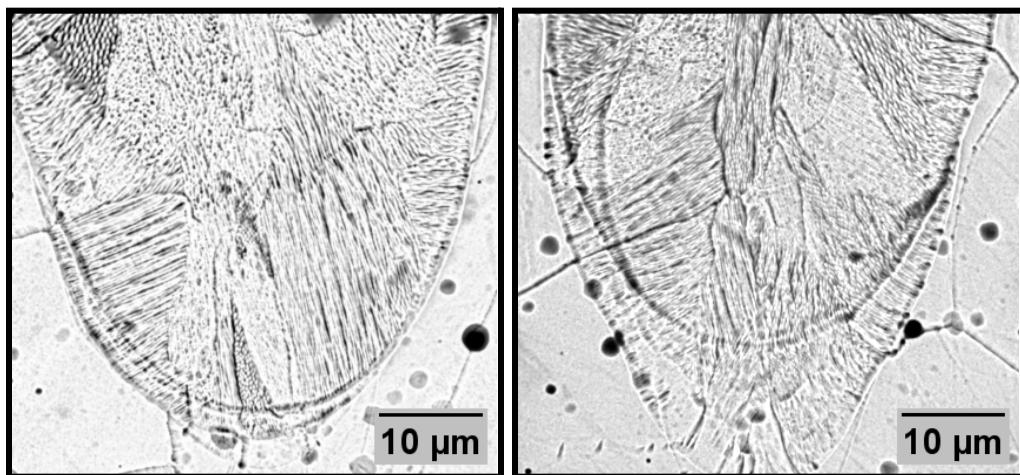


Figure 10: Left: 500 mm/s and Right: 1000 mm/s vapor convection tips that are enlarged to show the dark curves of banding and the sparsely-featured ghost-like areas.

Also of note in figure 3 is that, while there is a large mix of orientations, phases, and feature size, there are also some commonalities. For example, it appears that some areas

will have the same cooling rate, because the intercellular distance looks the same. In the same area, there is a mix of ferrite and austenite with about the same orientation, so the solidification velocity would need to be about the same. One of these areas is enlarged in figure 14. Hypothetically the convection could change the solute distribution to allow the difference in phase otherwise attributed to cooling rate or speed of solidification.

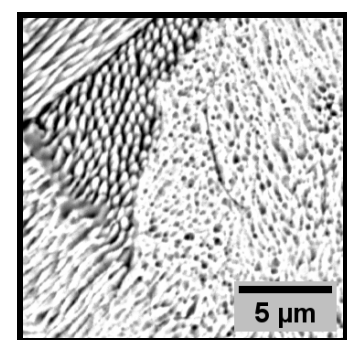


Figure 11: close up of the 500 mm/s region shown in figure 10 in order to highlight the austenite (white fingers in dark) and ferrite (dark holes in white) regions which appear to be a similar cell size and orientation.

## VALIDITY OF PLANE FRONT STABILITY CRITERION

The validity of the criterion is based upon the simplification of conditions to be conduction only, with minimal effects from convection. However, convection appears to overpower the

---

anticipated mechanisms at many points, even the carefully chosen locations shown in figure 1. The three melt tracks of a lower energy density showed the expected behavior. Namely,  $G/V$  at the surface should be lower than the criterion. The three higher energy density samples appeared to break that rule. The slower translation speed samples deviate from the conduction model in a number of ways, but the calculations used for this analysis made assumptions about the surface and fusion line which simply break down under convection. It is evident from looking at the figures above the difficulty in only measuring the cells distance between cells growing in the direction of translation, which is important when supposing translation velocity is solidification velocity. This lack of clear order for the slower translation speeds is not the only effect upon the deviation in the calculations, since solidification velocity must always be some non-zero component of the maximum translation velocity. This was an issue observed when calculating solidification velocities at the fusion line: the 0.5 mm/s track supposedly solidified at 4.9 mm/s and the 1 mm/s at 17 mm/s. Clearly, this does not match the expectation of a value less than  $V$  of laser, so the model likely does not fit. It is possible that a slight increase in thermal gradient is caused by the convection, or that the redistribution of solute from the convection creates a multivariable or differential equation defining a different  $G/V$  stability condition in a variety of compositions. For a more accurate analysis of the higher energy density samples, it could be interesting to propose a likely composition for the surface of each track based on available kinetic data, and calculate the plane front stability criterion under the approximation that the base metal is the supposed composition. Additionally, a larger number of samples could aid in the calculation of surface  $G$  since it is difficult to find clear features.